Laser-induced transfer of nanoparticles for gas-phase analysis

Laser-induced transfer of nanoparticles for gas-phase analysis

Alexander V. Bulgakov,[1,2,*] Nathan Goodfriend,[1] Oleg Nerushev,[1] Nadezhda M. Bulgakova,[2,3] Sergei V. Starinskiy,[2] Yuri G. Shukhov,[2] and Eleanor E. B. Campbell[1,4]

[1]*EaStCHEM, School of Chemistry, University of Edinburgh, Edinburgh EH9 3JJ, UK*
[2]*Institute of Thermophysics, Siberian Branch, Russian Academy of Sciences, Lavrentyev Ave. 1, 630090 Novosibirsk, Russia*
[3]*HiLASE Centre, Institute of Physics ASCR, Za Radnicí 828, 25241 Dolní Břežany, Czech Republic*
[4]*Department of Physics, Konkuk University, 143-701 Seoul, South Korea*
**Corresponding author: bulgakov@itp.nsc.ru*

Received June 2, 2014; revised August 13, 2014; accepted August 25, 2014; posted August 25, 2014 (Doc. ID 212813); published September 24, 2014

An experimental study of laser-induced forward transfer of nanoparticles from a metal-coated glass substrate is presented. Nanoparticles are efficiently removed from the substrates due to transient blister formation. A combination of mass spectrometry, atomic force microscopy studies of the irradiated substrates, and theoretical considerations of temperature distributions and stress in the films during irradiation serves to provide insight into the mechanisms involved.

OCIS codes: (310.6845) Thin film devices and applications; (320.2250) Femtosecond phenomena; (320.4240) Nanosecond phenomena; (350.1820) Damage; (350.3390) Laser materials processing.
http://dx.doi.org/10.1364/JOSAB.31.000C15

1. INTRODUCTION

The detection and characterization of isolated nanoparticles in the gas phase is an extremely challenging problem but of considerable importance for situations ranging from environmental monitoring to experiments that probe the foundations of physics [1,2]. A number of important analytical techniques for isolated particles, such as mass spectrometry and electron spectroscopy, require intact particles to be introduced into a region of high vacuum. One of the frequently used solutions is an aerodynamic lens system capable of delivering nanoparticles in a narrow beam into high vacuum [3,4]. However, the efficiency of this method drops dramatically for small particles (the critical size is ~30 nm), and the method also requires the initial aerosol formation. An alternative method for transferring nanoparticles into vacuum is matrix-assisted pulsed laser evaporation (MAPLE), which is based on the use of a highly absorbing, easily vaporized matrix (usually a polymer) that serves as a solvent for the analyte particles and, being vaporized, carries the analyte toward a detector [5,6]. Another laser-based method, laser-induced forward transfer (LIFT), is a noncontact, single-step, direct-write technique which employs pulsed laser radiation penetrating a transparent substrate to heat and vaporize a donor film deposited on it [7–11]. The transferred material is either spread on the film [9] or introduced into a matrix [10,11]. Both MAPLE and LIFT techniques can provide efficient and "mild" transfer of particles but also have drawbacks. First, the nanoparticles are transferred together with the absorbing matter, which is often unacceptable for analytical purposes. Another evident problem is the selection of an appropriate absorbing matrix. For studying large organic molecules, the matrix-assisted laser desorption/ionization technique has been developed, which is also based on the use of an absorbing matrix [12]. Direct laser desorption is a simple and efficient method for delivering particles for gas-phase analysis [13], but it usually results in heating, ionization, and fragmentation of the desorbed species.

Recently, a new matrix-free modification of the LIFT technique for nanoparticle transfer without destruction of the supporting film was proposed [14,15]. In this method, the nanoparticles are spread over a metal film deposited on a transparent substrate, and the interaction of a laser pulse with the metal–substrate interface causes, under certain conditions, transient blistering of the film, resulting in gentle transfer of nanoparticles without their heating. A variation of the blister-based LIFT method is acoustic wave-induced desorption, in which a thin metal foil is used instead of a coated transparent substrate [16,17]. The efficiency of these contamination-free techniques has been demonstrated for nanoparticle printing on a receiver substrate under standard air conditions [14,17–19] and for mass spectrometry of biomolecules [17]. We believe that this method can be very useful for transferring nanoparticles into analytical instruments for gas-phase analysis.

In this work, we have performed a study of blister-based laser-induced transfer under high-vacuum conditions for mass spectrometric analysis of gold-coated silica particles deposited on a thin titanium film. The gold nanoshells were detected at relatively large distances from the film, and their ejection velocities were measured. Based on an analysis of the laser-produced spots on the film using atomic force microscopy (AFM), we revealed two different regimes of blister formation and particle removal. Finally, we have performed a theoretical analysis of temperatures and mechanical stress realized in the irradiated titanium film under conditions of blister formation.

2. EXPERIMENTAL

The titanium films of 250 nm thickness were deposited by electron-beam evaporation (Nanospecs EBE-4 apparatus) onto glass microscope slides under ultrahigh vacuum conditions. As test nanoparticles we used well-characterized gold-coated silica particles (Nanospectra, 150 nm total diameter, 125 nm diameter of the silica core) in a water solution. The nanoparticles were deposited on the Ti films by a "sandwich" technique in which a droplet of the solution was squeezed-out between two substrates. The substrates were held together by surface tension, thus producing a uniform liquid layer. Low heat was then applied to the bottom substrate to evaporate the water. By using this procedure several times we were able to produce a relatively uniform film of isolated nanoparticles over an area of 400 mm^2 with a particle surface density of around 2×10^6 mm^{-2}. The film with nanoparticles was placed in a high vacuum chamber (base pressure 3×10^{-7} mbar) on a two-dimensional translation stage and irradiated through the substrate by a pulse of a Nd:YAG laser (532 nm wavelength, 5 ns pulse duration) to produce a Gaussian spot of 200–300 μm in diameter. The peak laser fluence at the film–substrate interface was varied in the range 200–400 mJ/cm^2 that covered the range of irradiation conditions from the threshold of particle LIFT to Ti film ablation.

The transferred nanoparticles were investigated in the gas phase by laser ablation time-of-flight mass spectrometry (TOF MS). Details of the MS measurements will be described elsewhere [20]. Here we briefly outline the experiments. Two MS apparatus with different extraction geometries and ionization methods were used. In the first one, the removed nanoparticles were allowed to travel 8 mm before entering a constant extraction field directed along the particle flight. At a distance of 16 mm from the film the particles were irradiated by a 120 fs pulse from a frequency-doubled Ti:sapphire laser (400 nm) at a 45° incidence angle to the particle flight direction and at a variable time delay t after the nanosecond desorption pulse. The produced positive ions were analyzed by a linear TOF MS. Preliminary experiments of femtosecond-laser ablation of a sandwich metal film (50-nm gold film with a 20-nm titanium sublayer on a glass substrate) placed at the point of particle ionization were performed to optimize irradiation and detection conditions for the highest ion signal in the MS. A femtosecond-laser fluence of ~300 mJ/cm^2 was chosen for irradiating the particles removed from the substrate in the LIFT experiments as it resulted in complete ablation of the gold film by a single pulse with a fairly high ion yield. In the second MS apparatus [21], nanoparticles traveled over a distance of 36 mm toward a repeller grid where they were ablated at a corresponding time delay by 193-nm photons (5-ns pulse of a ArF laser at ~1 J/cm^2). The produced ions were extracted with a perpendicular geometry and analyzed by a reflectron TOF MS. Variation of the time delay t between the LIFT laser pulse and postionization laser pulse (either femtosecond or nanosecond) allowed us to characterize the velocities of the desorbed nanoparticles.

All experiments were performed for single-pulse conditions. After every pulse, the substrate with nanoparticles was translated to expose a new site of the film to the next nanosecond-laser pulse. The positions of the produced spots were fixed so that direct comparison of a particular mass spectrum with an image of the corresponding spot could be made. The film surface after irradiation was analyzed by AFM (Nanoman-V) equipped with a variable magnification optical system.

3. RESULTS AND DISCUSSION

The LIFT-ejected nanoparticles were detected with both MS apparatus. Figure 1(a) shows a typical mass spectrum obtained with femtosecond-laser ionization. As the used intensity of the femtosecond-laser pulse corresponds to a deep ablation regime, all constituents of the nanoparticles are observed in the mass spectrum. The main peak corresponds to $SiOH^+$, the most stable cation produced in ion–molecule reactions of Si^+ and SiO^+ ions, which originate from the particle core, with hydrogen and water molecules present as a background in the vacuum chamber [22]. In contrast to the broad background peaks, the $SiOH^+$ peak is narrow [Fig. 1(a)] since these ions are produced at a fixed point of crossing of the laser and nanoparticle beams and thus have a fixed flight energy while the background ions are generated with broad energy distributions for our 45 deg angle ionization geometry. There is a relatively low yield of Au^+ ions under these conditions (not shown), possibly due to the fact that the ultrashort laser ablation of the gold shell occurs predominantly, under these conditions, through a spallation mechanism [23,24]

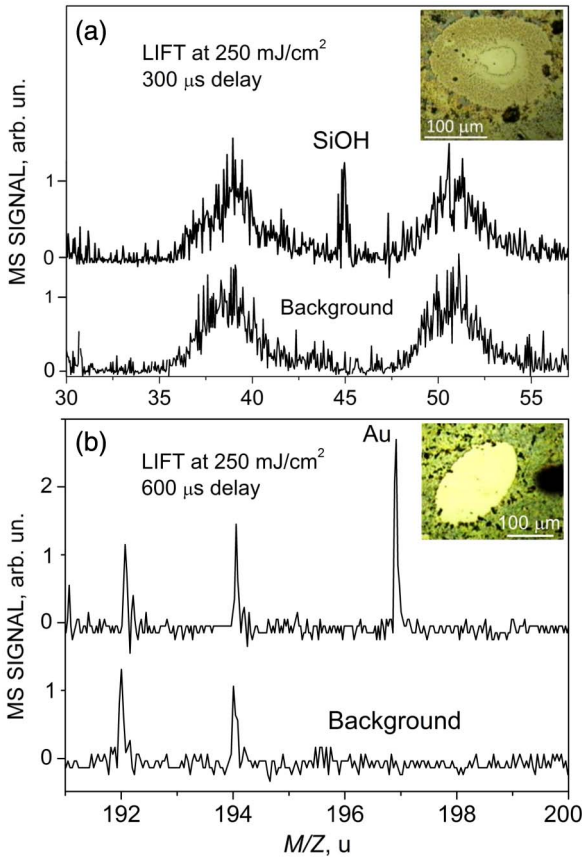

Fig. 1. Mass spectra of positive ions produced by irradiation of ejected gold-coated silica nanoparticles with (a) femtosecond-laser pulse at 400 nm and (b) nanosecond-laser pulse at 193 nm at time delays corresponding to particle velocity of (a) 50 m/s and (b) 60 m/s. The ejection was induced by a 532-nm, 5-ns laser at 250 mJ/cm^2. The bottom panels are background mass spectra when the LIFT laser pulse is not applied. The insets are the corresponding spot images.

when fragments of the shell are mechanically removed without formation of the vapor or plasma phase. The Au^+ peaks are more pronounced in the mass spectrum with ionization by UV nanosecond-laser pulses [Fig. 1(b)] when a thermal ablation mechanism appears to dominate.

For both MS arrangements, the nanoparticles were observed in relatively narrow ranges of time delay t, corresponding to typical particle velocities of ~50 m/s. This value is in good agreement with available data for the maximum ejection velocity in the blistering regime evaluated as ~100 m/s from shadow graphic imaging of diamond nanopowder transferred by picosecond LIFT [25]. Also, nearly the same value (~60 m/s) was obtained for the maximum movement velocity of a 200-nm SnO_2 film in simulations of blister formation under irradiation conditions similar to ours [26]. The corresponding kinetic energy of our transferred nanoparticles in the gas phase is around 100 keV (calculated assuming bulk densities for gold and silica). Thus, thermal desorption of nanoparticles from the substrate can be definitely ruled out.

By comparing the obtained mass spectra with the corresponding spot images we have found that the particle ejection is observed in our experiments when the film remains undamaged without any cracks in the spot. The insets in Figs. 1(a) and 1(b) show optical images of the spots that resulted in the corresponding mass spectra. The maximum concentration of nanoparticles in the MS extraction region was observed to be obtained for nanosecond laser fluences close to, but still below, the threshold for film cracking.

Under our experimental conditions we produced basically two kinds of spots (typical examples are shown in Fig. 2). At low fluences (200–280 mJ/cm^2), the spot remains flat after radiation with a clear boundary, indicating efficient removal of nanoparticles from the film within the spot. Near, but below, a threshold fluence of ~280 mJ/cm^2 the spot consists of two regions, again with a clear boundary between the regions [Fig. 2(a)]. Such kinds of spot resulted in the strongest MS signals. We assume, as in [15,19,26], that the particles are ejected due to formation of a transient blister in the Ti film, and its deformation is elastic so the film returns to the original position after cooling down and release of the temperature-induced mechanical stress. We also assume that formation of the central zone is due to film melting (see discussion below).

At laser fluences slightly exceeding the threshold value, the spot images are completely different. Multiple cracks and bumps are produced in the film, resulting in a flower structure of the spot [Fig. 2(b)]. Obviously, the elastic deformation limit was exceeded during blister formation in this case, and the brittle Ti film was heavily damaged. Similar flower-like structures produced due to exceeding the stress limit in the film were recently observed by ultrafast pump-probe microscopy [27]. Note that nanoparticles were efficiently removed from this kind of spot as well, as seen from Fig. 2(b). However, the intensity of the signal in the mass spectrum, at the same extraction conditions used to obtain Fig. 1, was considerably lower, indicating a significantly different velocity and/or angular distribution. For instance, the nanoparticles can be released in all directions from such a cracked spot and thus have a broader angular distribution than from the flat undamaged spot when nanoparticles are essentially transferred in the forward direction. As a result, the nanoparticle density

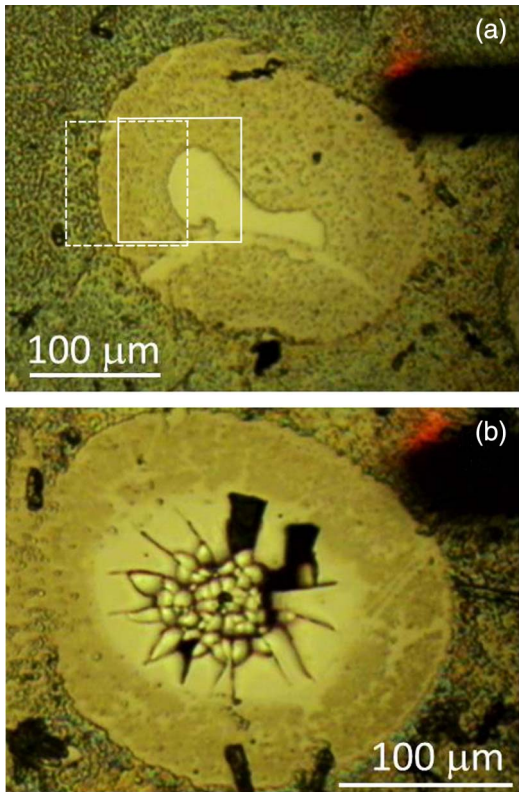

Fig. 2. Typical optical images of LIFT-produced spot at (a) 250 mJ/cm^2 (no film damage, high efficiency of particle transfer to MS) and (b) 320 mJ/cm^2 (film cracking, low efficiency of particle transfer). The outlined square regions in Fig. 2(a) are shown in more detail in Figs. 3 and 4.

becomes too low at the distance of their mass spectrometric detection. This hypothesis remains to be tested experimentally.

Figures 3 and 4 show more detailed images and surface height profiles obtained with AFM for the spot produced under near-threshold conditions [Fig. 2(a)]. As seen, the central zone of the spot is completely clean of the nanoparticles, and its profile is almost flat (Fig. 3) while there are some particles left in the external zone (Fig. 4). According to AFM measurements, the average surface density of the particles remaining in the external zone is $\sim 3 \times 10^5$ mm^{-2}; that is, about 85% of nanoparticles were removed from the external zone. The height profile across the external zone indicates that the central zone is slightly lifted (~60 nm) with respect to the baseline level in the undamaged area, which presumably corresponds to the original film surface. This means that the blister did not return back completely, and the central part of the film is slightly delaminated.

An interesting feature of Fig. 3 is the structure of the boundary between the central and external zones. The boundary represents a line made of individual nanoparticles with almost no gaps between them. Its height corresponds to the particle size, and in some places there are two or more particles aggregated. It looks as if all the particles remaining on the surface after the LIFT process were pushed toward the boundary of the central molten zone. A rough estimate of the area and boundary of the central spot shows that ~1600 close-packed particles would be needed to form the boundary ring. This corresponds to ~20% of the particles that were originally

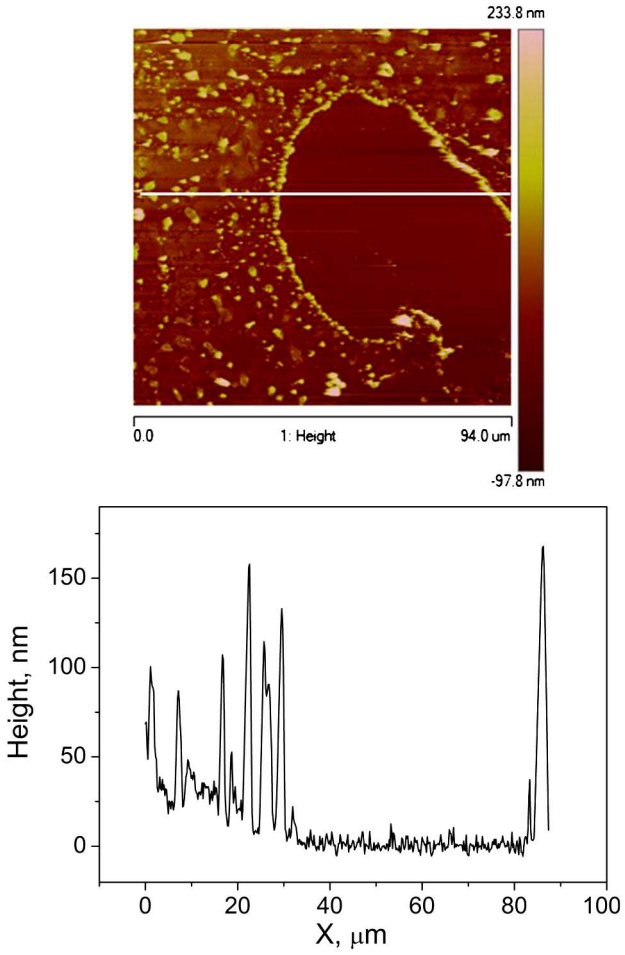

Fig. 3. (Top) AFM image and (bottom) surface height profile for the central zone of the LIFT-produced spot within the square area outlined in Fig. 2(a) by the solid line. The profile is taken for the cross section shown by the straight line. The higher peak on the right-hand side can be due to an aggregate of two nanoparticles.

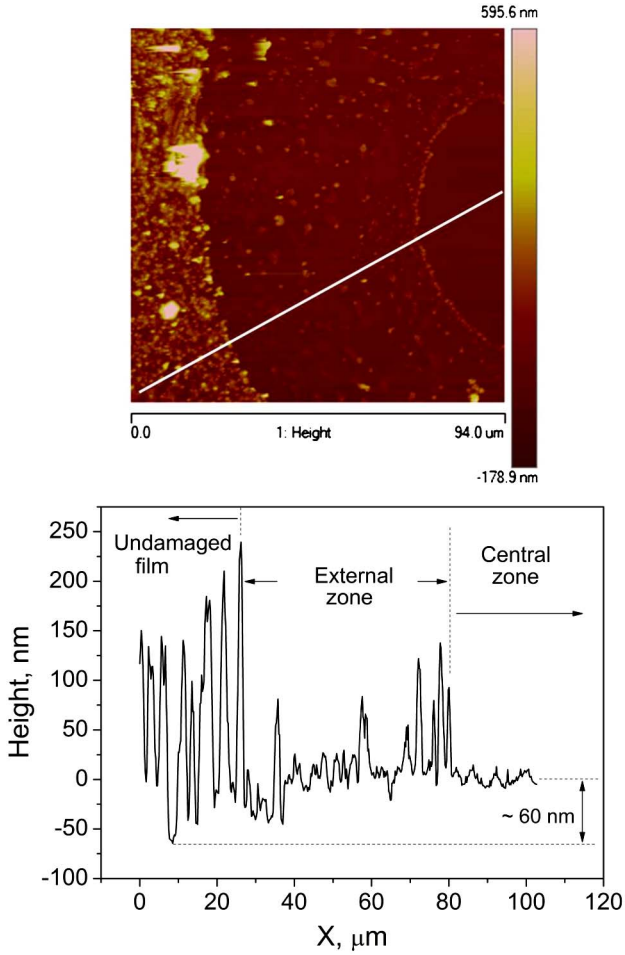

Fig. 4. Same as in Fig. 3 but for the external zone of the spot [the region is shown in Fig. 2(a) by the dashed line].

present in the central region, in good agreement with the percentage of particles remaining in the external zone.

To get a more detailed insight into the processes occurring under blister-based LIFT of nanoparticles, we have made estimations of laser-induced thermal stress in the titanium films under our irradiation conditions and associated film distortion which is responsible for the nanoparticles being desorbed from the film surface. For the estimations we use approaches proposed in [26,28]. It is assumed that the film is suddenly heated uniformly through its thickness. Radially, in the absence of ablation, the film temperature has a Gaussian profile reflecting the radial beam shape. As a result of heating and associated thermal expansion, the hot part of the film experiences high thermal stress, the maximum value of which may be evaluated based on the approximate solution of the thermoelasticity problem for a uniformly heated round plate with fixed edges [28]:

$$\sigma_{r\,\max} = \frac{E k_e \Delta T}{2(1-\nu)}, \tag{1}$$

where E is the Young's modulus, k_e is the coefficient of linear thermal expansion, ν is the Poisson ratio, and ΔT is the temperature rise in the film.

To proceed with estimations of the maximum thermal stress generated in the film upon laser heating, we have to evaluate the film temperature. As metals have high thermal conductivities while the substrate is made of low-heat-conducting glass, one may consider that the film is rapidly heated uniformly across the film thickness and disregard heat exchange with the substrate, at least during the first several tens of nanoseconds [26]. Due to the large irradiation spot radius relative to the film thickness, we can also disregard radial heat conduction on such temporal scales. Under such assumptions, all heat absorbed by the film is used for local heating of the film within the irradiation spot. Then one may write for the maximum temperature that is reached in the center of the irradiation spot,

$$T_{\max} = T_0 + \frac{(1-R)F_0}{c_p d}, \tag{2}$$

where c_p is the heat capacity, d is the film thickness, R is the reflection coefficient, F_0 is the peak laser fluence, and T_0 is the initial (room) temperature. For 532 nm laser wavelength, the titanium optical constants are $n = 1.86$, $k = 2.88$ [29], giving $R = 0.548$. With $c_p = 2.36\ \mathrm{J/(cm^3\,K)}$ as for bulk titanium, we obtain for the spots shown in Fig. 2 $T_{\max} \approx 2220$ K at $F_0 = 250\ \mathrm{mJ/cm^2}$ and 2760 K at

$F_0 = 320$ mJ/cm^2, that is, above the melting point $T_{melt} = 1941$ K in both cases. However, taking into account the heat of fusion ($\Delta H_{melt} = 14.15$ kJ/mol) implies that at 250 mJ/cm^2 the temperature does not exceed T_{melt}, and the film at the center of the spot remains incompletely molten. At 320 mJ/cm^2, the film temperature at the center of the spot exceeds the melting point and reaches $T_{max} \approx 2200$ K.

To estimate the thermal stress for our nonuniformly heated film, we assume that the average ΔT value is approximately equal to $\Delta T_{max}/2$. Then, based on the tabulated thermal and mechanical properties of titanium ($k_\varepsilon = 8.6 \times 10^{-6}$ K^{-1}, $E = 116$ GPa, and $\nu = 0.32$), Eq. (1) gives ~600 and 700 MPa, respectively for 250 and 320 mJ/cm^2. Both these values exceed the tensile strength of bulk titanium (~434 MPa [30]). It must also be mentioned that the tensile strength of materials may decrease upon heating. However, it is known that upon dynamic loading, materials withstand stress levels much higher than do the static ones, which can explain the absence of cracks for 250 mJ/cm^2 where the stress value is estimated to be ~38% higher than the tensile strength. At the higher laser fluence of 320 mJ/cm^2 the estimated stress exceeds the tensile strength by more than 60%. Even if the central part of the irradiation spot is heated above the melting point, the large ring area beyond the molten zone remains under stress and may crack. It is important to underline that in [28] titanium is classified as a material of low plasticity, which is not suitable for micro- and nanotexturing due to its tendency to fail/crack but not to deform. It is also important that the laser-induced stress at 250 mJ/cm^2 is below the yield stress for thin titanium films (~700 MPa [31]). This means that the film does not exceed the elastic deformation limit during blister formation and returns back after nanoparticle emission, as observed in our experiments (Figs. 3 and 4).

Under large stress loads the film experiences bulging off the substrate, while beyond the irradiation spot it stays attached to the substrate [26,28,32]. Similarly to [26], we assume that the bump represents a segment of a sphere of radius R (see Fig. 5), which can be characterized by the angle of curvature θ. Then the height h of the bump can be estimated as

$$h = r(1 - \cos(\theta))/\sin(\theta), \tag{3}$$

where the angle θ is evaluated geometrically through the thermal expansion of the film,

$$\theta/\sin(\theta) = 1 + k_\varepsilon \Delta T. \tag{4}$$

This gives h values of 11 and 12.6 μm for 250 and 320 mJ/cm^2, respectively.

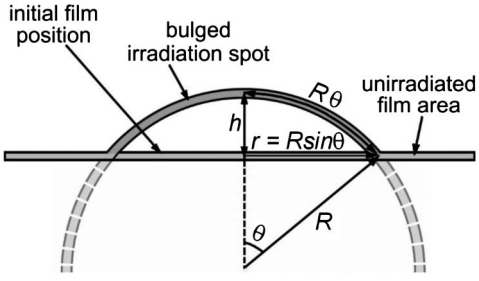

Fig. 5. Schematics of film bulging (adapted from [26]). For details see the text.

After bulging, if the film stays below both the elastic limit and tensile strength, it returns back to the substrate being uncracked [Fig. 2(a)]. If the elastic limit is exceeded, the film is plastically deformed, and a permanent bump is formed, as observed for plastic materials [32]. A third situation is inherent for materials with low plasticity, in particular metals including titanium, as discussed in [28]. Films of such materials will be either destroyed by ejecting solid pieces [33,34] or return back to the substrate, preserving the evident crack patterns as in Fig. 2(b) at 320 mJ/cm^2. Assuming that the detected nanoparticles received momentum from the film, we can estimate that a film with a velocity of ~50 m/s will be deformed by 11–13 μm during approximately 200–250 ns. Hence, the film returns back to the substrate in less than a half of a microsecond.

In order to understand the formation of the nanoparticle ring around the boundary between the central and external zones we consider the dynamics of the molten zone. One can estimate that to heat the 250 nm thick film to its melting point (without accounting for heat required for the melting process) the laser fluence $F_0 \approx 215$ mJ/cm^2, corresponding to an absorbed fluence of 97 mJ/cm^2, should be applied. From the Gaussian spatial profile of the laser, the radius of the film region heated to the melting point is ~40 and 64 μm for the two laser fluences of Fig. 2. Even a partially melted region can experience convective motion known as the Marangoni effect [35] as illustrated in Fig. 6. The film is shown schematically after bulging and subsequent return to the substrate. Nanoparticles are essentially emitted from the deformed area of the film while they are preserved at the unirradiated film regions. The essence of the Marangoni effect which develops in the molten (or partially molten) film region is that on a free liquid surface with a temperature gradient, shear stress is developed, pushing the liquid to flow toward the regions with larger surface tension (or lower temperature for most liquid substances). Evidently, if not all nanoparticles have been lifted during the film deformation process, those which remain in the molten region will be dragged toward the liquid–solid boundary and accumulate at the boundary. Hence, the appearance of the nanoparticle ring around the center of the irradiation spot may be attributed to the boundary of the molten phase. It thus appears that nanoparticles deposited on a solid surface may be used as markers indicating the boundaries of the molten region. Note that in our case the film can stay molten up to several microseconds as extraction of heat from the film by the glass substrate is a slow process (typical velocity of the heat wave front in glass is 1 μm per 1 μs) while the radial thermal conductivity within the 250-nm titanium film can be neglected for our spot sizes.

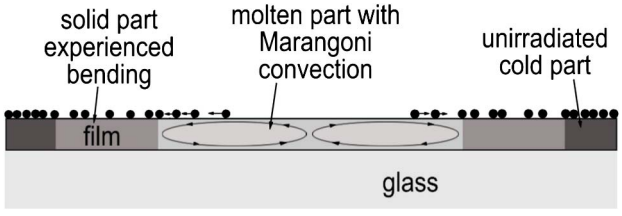

Fig. 6. Schematics of Marangoni convection in the molten part of the film which moves the remaining nanoparticles to the edges of the molten zone, creating the nanoparticle ring.

It might appear surprising at first sight that the molten titanium film, which experiences the Marangoni convection, remains nearly flat after solidification. Indeed, a number of previous works indicate that laser-induced melting of metal films results in formation of various protrusions on the film surface [36–38]. However, with our relatively large spot sizes (at least an order of magnitude larger than those used in these works), the parameter gradients along the surface are much smaller, resulting in a slow "laminar" convection flow and in a smooth melt profile [39]. In addition, the surface topography development is strongly dependent on the thickness and material of the film as well as on the underlying substrate. For example, Camacho-López *et al.* [40] show that periodic structures are observed when irradiating thin Ti films on Si with nanosecond laser pulses but not when the Ti thin film is deposited on glass (the substrate that we use here). Therefore, the absence of considerable residual deformation of the titanium film after being molten under our irradiation conditions is not very surprising. On the other hand, experiments under identical conditions on Ti films without deposited nanoparticles that can mask any small changes show a slight change of height (10–20 nm) around the position of the central boundary region, providing support for the assumption that the region has undergone melting and the development of a flow of molten material [20].

4. CONCLUSIONS

We have considered the use of thin Ti films deposited on glass as a suitable substrate for laser-induced transfer of nanoparticles. A combination of experimental studies of nanoparticle velocity, substrate deformation, and density of nanoparticles remaining on the irradiated samples as well as theoretical considerations of temperature and stress build-up in the irradiated thin films provides insight into the mechanisms of particle removal. The Marangoni effect has been invoked to explain the formation of a well-defined boundary region consisting of a ring of densely packed nanoparticles surrounding a central zone that has been emptied of nanoparticles during the LIFT process. Further experiments are underway to test the interpretation of results that is presented here.

ACKNOWLEDGMENTS

The authors thank J. O. Johansson for his help with femtosecond-laser operation and useful discussions. This research is supported by Marie Curie International Incoming Fellowship grant No. 302991. A. V. Bulgakov, S. V. Starinskiy, and Y. G. Shukhov acknowledge support from the SBRAS (Integration Project No. 134). N. M. Bulgakova acknowledges co-financing by the European Regional Development Fund, the European Social Fund, and the state budget of the Czech Republic (project HiLASE: CZ.1.05/2.1.00/01.0027, project DPSSLasers: CZ.1.07/2.3.00/20.0143), and grant RVO 68407700.

REFERENCES

1. P. Biswas and C.-Y. Wu, "Nanoparticles and the environment," J. Air Waste Managem. Assoc. **55**, 708–746 (2005).
2. T. Juffmann, S. Truppe, P. Geyer, A. G. Major, S. Deachapunya, H. Ulbricht, and M. Arndt, "Wave and particle in molecular interference lithography," Phys. Rev. Lett. **103**, 263601 (2009).
3. P. S. K. Liu, R. Deng, K. A. Smith, L. R. Williams, J. T. Jayne, M. R. Canagaratna, K. Moore, T. B. Onasch, D. R. Worsnop, and T. Deshler, "Transmission efficiency of an aerodynamic focusing lens system: comparison of model calculations and laboratory measurements for the aerodyne aerosol mass spectrometer," Aerosol Sci. Technol. **41**, 721–733 (2007).
4. M. R. Canagaratna, J. T. Jayne, J. L. Jimenez, J. D. Allan, M. R. Alfarra, Q. Zhang, T. B. Onasch, F. Drewnick, H. Coe, A. Middlebrook, A. Delia, L. R. Williams, A. M. Trimbom, M. J. Northway, P. F. DeCarlo, C. E. Kolb, P. Davidovits, and D. R. Worsnop, "Chemical and microphysical characterization of ambient aerosols with the aerodyne aerosol mass spectrometer," Mass Spectrom. Rev. **26**, 185–222 (2007).
5. D. B. Chrisey, A. Piqué, R. A. McGill, J. S. Horwitz, B. R. Ringensen, D. M. Bubb, and P. K. Wu, "Laser deposition of polymer and biomaterial films," Chem. Rev. **103**, 553–576 (2003).
6. A. Piqué, "The matrix-assisted pulsed laser evaporation (MAPLE) process: origins and future directions," Appl. Phys. A **105**, 517–528 (2011).
7. J. Bohandy, B. F. Kim, and F. J. Adrian, "Metal deposition from a supported metal film using an excimer laser," J. Appl. Phys. **60**, 1538–1539 (1986).
8. I. Zergioti, S. Mailis, N. A. Vainos, C. Fotakis, S. Chen, and C. P. Grigoropoulos, "Microdeposition of metals by femtosecond excimer laser," Appl. Surf. Sci. **127–129**, 601–605 (1998).
9. B. Hopp, T. Smausz, Z. Antal, N. Kresz, Z. Bor, and D. Chrisey, "Absorbing film assisted laser induced forward transfer of fungi (Trichoderma conidia)," J. Appl. Phys. **96**, 3478–3481 (2004).
10. J. A. Barron, B. J. Spargo, and B. R. Ringeisen, "Biological laser printing of three dimensional cellular structures," Appl. Phys. A **79**, 1027–1030 (2004).
11. M. Nagel, R. Fardel, P. Feurer, M. Haberl, F. Nuesch, T. Lippert, and A. Wokaum, "Aryltriazene photopolymer thin films as sacrificial release layers for laser-assisted forward transfer system: study of photoablative decomposition and transfer behavior," Appl. Phys. A **92**, 781–789 (2008).
12. A. Vertes, R. Gijbels, and F. Adams, eds., *Laser Ionization Mass Analysis* (Wiley, 1993).
13. T. Laitinen, K. Hatonen, M. Kulmala, and M.-L. Riekkola, "Aerosol time-of-flight mass spectrometer for measuring ultrafine aerosol particles," Boreal Environ. Res. **14**, 539–549 (2009).
14. T. V. Kononenko, P. Alloncle, V. L. Konov, and M. Sentis, "Laser transfer of diamond nanopowder by metal film blistering," Appl. Phys. A **94**, 531–536 (2009).
15. M. S. Brown, N. T. Kattamis, and C. B. Arnold, "Time-resolved study of polyimide absorption layers for blister-actuated laser-induced forward transfer," J. Appl. Phys. **107**, 083103 (2010).
16. V. Menezes, K. Takayama, T. Ohki, and J. Gopalan, "Laser-ablation-assisted microparticle acceleration for drug delivery," Appl. Phys. Lett. **87**, 163504 (2005).
17. C. R. Calvert, L. Belshaw, M. J. Duffy, O. Kelly, R. B. King, A. G. Smyth, T. J. Kelly, J. T. Costello, D. J. Timson, W. A. Bryan, T. Kierspel, P. Rice, I. C. E. Turcu, C. M. Cacho, E. Springate, I. D. Williams, and J. B. Greenwood, "LIAD-fs scheme for studies of ultrafast laser interaction with gas phase biomolecules," Phys. Chem. Chem. Phys. **14**, 6289–6297 (2012).
18. T. V. Kononenko, I. A. Nagovitsyn, G. K. Chudinova, and I. N. Mihailescu, "Application of clean laser transfer for porphyrin micropatterning," Appl. Sur. Sci. **256**, 2803–2808 (2010).
19. T. Mattle, A. Hintennach, T. Lippert, and A. Wokaun, "Laser induced forward transfer of SnO_2 for sensing applications using different precursors systems," Appl. Phys. A **110**, 309–316 (2013).
20. A. V. Bulgakov (School of Chemistry, University of Edinburgh, Edinburgh EH9 3JJ, UK) N. Goodfriend, T. Ridley, Yu. G. Shukhov, and E. E. B. Campbell, are preparing a manuscript to be called "A mass spectrometric study of blister-based laser-induced transfer of nanoparticles."
21. A. V. Bulgakov, A. B. Evtushenko, Yu. G. Shukhov, I. Ozerov, and W. Marine, "Pulsed laser ablation of binary semiconductors: mechanisms of vaporization and cluster formation," Quantum Electron. **40**, 1021–1033 (2010).
22. S. Wlodek, A. Fox, and D. K. Bohme, "Gas-phase reactions of Si^+ and $SiOH^+$ with molecules containing hydroxyl groups: possible ion–molecule reactions pathways toward silicon monoxide, silanoic acid, and trihydroxy-, trimethoxy-, and triethoxysilane," J. Am. Chem. Soc. **109**, 6663–6667 (1987).

23. B. J. Demaske, V. V. Zhakhovsky, N. A. Inogamov, and I. I. Oleynik, "Ablation and spallation of gold films irradiated by ultrashort laser pulses," Phys. Rev. B **82**, 064113 (2010).
24. Y. Gan and J. K. Chen, "An atomic-level study of material ablation and spallation in ultrafast laser processing of gold films," J. Appl. Phys. **108**, 103102 (2010).
25. T. V. Kononenko, P. Alloncle, V. L. Konov, and M. Sentis, "Shadowgraphic imaging of laser transfer driven by metal film blistering," Appl. Phys. A **102**, 49–54 (2011).
26. Yu. P. Meshcheryakov, M. V. Shugaev, T. Mattle, T. Lippert, and N. M. Bulgakova, "Role of thermal stresses on pulsed laser irradiation of thin films under conditions of microbump formation and nonvaporization forward transfer," Appl. Phys. A **113**, 521–529 (2013).
27. S. Rapp, J. Rosenberger, M. Domke, G. Heise, H. P. Huber, and M. Schmidt, "Ultrafast pump-probe microscopy reveals the mechanism of selective fs laser structuring of transparent thin films for maskless micropatterning," App. Surf. Sci. **290**, 368–372 (2014).
28. Y. P. Meshcheryakov and N. M. Bulgakova, "Thermoelastic modeling of microbump and nanojet formation on nanosize gold films under femtosecond laser irradiation," Appl. Phys. A **82**, 363–368 (2006).
29. E. D. Palik, *Handbook of Optical Constants of Solids* (Academic, 1998).
30. "Introduction to titanium," http://www.titaniferous.com/introduction-to-titanium.
31. Z. Shan and S. K. Sitaraman, "Elastic–plastic characterization of thin films using nanoindentation technique," Thin Solid Films **437**, 176–181 (2003).
32. F. Korte, J. Koch, and B. N. Chichkov, "Formation of microbump and nanojets on gold targets by femtosecond laser pulses," Appl. Phys. A **79**, 879–881 (2004).
33. K. Sokolowski-Tinten, W. Ziegler, D. von der Linde, M. P. Siegal, and D. L. Overmyer, "Short-pulse-laser-induced optical damage and fracto-emission of amorphous, diamond-like carbon films," Appl. Phys. Lett. **86**, 121911 (2005).
34. P. Gecys, E. Markauskas, M. Gedvilas, G. Raciukaitis, I. Repins, and C. Beall, "Ultrashort pulsed laser induced material lift-off processing of CZTSe thin-film solar cells," Solar Energy **102**, 82–90 (2014).
35. J. Svensson, N. M. Bulgakova, O. A. Nerushev, and E. E. B. Campbell, "Marangoni effect in SiO_2 during field directed chemical vapor deposition growth of carbon nanotubes," Phys. Rev. B **73**, 205413 (2006).
36. D. A. Willis and X. Xu, "Transport phenomena and droplet formation during pulsed laser interaction with thin films," J. Heat Transfer **122**, 763–770 (2000).
37. A. I. Kuznetsov, J. Koch, and B. N. Chichkov, "Nanostructuring of thin gold films by femtosecomd lasers," Appl. Phys. A **94**, 221–230 (2009).
38. J. P. Moening, S. S. Thanawala, and D. G. Geprgiev, "Formation of high-aspect-ratio prostrations on gold films by localized pulsed laser irradiation," Appl. Phys. A **95**, 635–638 (2009).
39. D. Bäuerle, "Surface melting," in *Laser Processing and Chemistry* (Springer-Verlag, 2000), pp. 190–193.
40. S. Camacho-López, M. A. Camacho-López, O. O. Mejía, R. Evans, G. C. Vega, M. A. Camacho-López, M. H. Zaldivar, A. E. García, and J. G. B. Muñetón, "Processing of metallic thin films using Nd:YAG laser pulses," in *Nd YAG Laser*, D. C. Dumitras, ed. (InTech, 2012), pp. 23–40.